# EXPERIENCE WITH A DOUBLE HARDENING MODEL FOR SOIL

D.V. Griffiths[1] and I.M. Smith[2]

[1]Lecturer, [2]Reader,
University of Manchester, England

SUMMARY. Experience of evaluating a typical double-hardening model for soil on various non-cyclic stress paths is described. Loose and dense materials following drained (including $K_o$) and undrained paths are dealt with. The stress-strain response is embedded within a finite element program so that direct application to boundary value problems is feasible. Remarks are made about potentially interesting problems which could benefit from such complicated treatment and about the relationships between "sands" and "clays".

## INTRODUCTION

Recent work on constitutive models for soil has been concentrated on the description of behaviour under cyclic loadings, for example (1). This has obvious potential application to the prediction of soil behaviour in earthquakes but it seems to be a paradox that such complicated boundary value problems are being considered before any significant examination of the response of soil masses under non-cyclic conditions. At a recent workshop (2) some twelve constitutive models for soil were compared over various simple stress paths applied to elements of "kaolinite", "sand", "clay X" and "clay Y". Even these test conditions were quite restrictive in that only the kaolinite was examined in the undrained state whereas the others were all fully drained. Nevertheless the predictions of the twelve models were quite variable. What emerged was that for many practical purposes a rather simple model such as that of Duncan and Chang (3) is quite adequate. Under similar conditions the authors' preference would be for a simple elastoplastic model, eg. Griffiths (4), but this is a matter of detail.

What is really required in practice is that problems be identified in which the use of such simple models would seriously fail to account for the main physical phenomena under investigation. An attempt to list some of these has recently been made (5) in relation to boundary value problems involving sands. For these special situations a typical double hardening model, Molenkamp (6), has been implemented and shown to account for the effective stress-strain-volume change (porewater pressure) response of dense sand. The model is closely allied to other double hardening models, eg. Lade (7), but does not appeal to kinematic hardening, eg. Ghaboussi and Momen (8) or Mroz and St Pietruszczak (9). Nor is it based on "critical state" concepts, eg. Nova (10).

In the present paper, previous results for dense sand following mainly drained stress paths are augmented by results for loose sands and for undrained stress paths. The $K_o$ condition is also investigated.

A feature of the results presented is that the governing equations were integrated within a typical finite element program so that rapid extension to the solution of boundary value problems is feasible.

In the next section, the essential features of the model will briefly be reviewed, and in the subsequent section the finite element implementation will be outlined. Thereafter the results for the various materials and stress paths will be discussed.

## SUMMARY OF THE MODEL

For a detailed description, the interested reader should refer to Molenkamp (6), but the basic features will be described here.

In its fullest form the model requires 21 parameters for its definition, but due either to lack of data or insufficient quality data, the values assigned to several of the parameters cannot be established with great confidence. In the absence of highly detailed experimental observation, it has been

noted (5) that the number of "important" parameters could be reduced to 10 or even 4.

The model used in the present work is typical of the double hardening type, and has many points in common with the models of Lade (7) and Vermeer (11). The present model has greater versatility in its ability to make fine adjustments to the stress-strain law, but these are at the expense of more governing parameters, and greater reliance on high quality test data.

The model uses concepts of plasticity theory to generate irrecoverable strains during loading and has utilised curve fits to the work of Rowe (12,13), Tatsuoka and Ishihara (14), Lade (7), Vermeer (11) and Yamada and Ishihara (15).

Increments of strain are split into three components: elastic, isotropic plastic and deviatoric plastic, and the number of parameters required to describe these are in the ratio 3:2:16 which reflects the complexity of shear-dilatancy coupling in granular soil. Although the present model, in line with current trends, uses two distinct yield surfaces for isotropic and deviatoric loading it may be that a single smooth surface could cope with both effects as has been suggested by Smith (16). It should be remembered that although yield is treated in a similar way mathematically on both surfaces, failure of the soil can only be caused by shear where the failure surface represents the outermost shear yield surface. Isotropic compression alone, although causing yield, can never result in failure; indeed it strengthens the soil.

Although the parameters required for the model can all be obtained from triaxial tests, all formulations are in terms of invariants to facilitate use with general stress states.

For example the isotropic and deviatoric stress invariants are respectively:

$$s = \frac{1}{\sqrt{3}} (\sigma_1 + \sigma_2 + \sigma_3) \qquad (1)$$

$$t = \frac{1}{\sqrt{3}} ((\sigma_1 - \sigma_2)^2 + (\sigma_2 - \sigma_3)^2 + (\sigma_3 - \sigma_1)^2)^{\frac{1}{2}} \qquad (2)$$

The strain invariant counterparts v and $\gamma$ are of the same form except with principal strains $\varepsilon_1, \varepsilon_2$ and $\varepsilon_3$ replacing the principal stresses.

## Elastic Model

The non-linear elastic model is based on a constant Poisson's ratio and a stress-dependent shear modulus after Vermeer (11). This leads to the isotropic stress and elastic strain being related by the power law:

$$v^e = A(\frac{s}{p_A})^{AP} \qquad (3)$$

where A, AP are model parameters and $p_A$ is atmospheric pressure used to non-dimensionalise the equation.

## Plastic Model

Both plastic strain increments, namely $d\varepsilon_{ij}^c$ due to the compressive model, and $d\varepsilon_{ij}^d$ due to the deviatoric model are calculated by the general expression for plastic strain:

$$d\varepsilon_{ij} = \frac{\frac{\partial G}{\partial \sigma_{ij}} \frac{\partial F}{\partial \sigma_{kl}} d\sigma_{kl}}{H} \qquad (4)$$

in which F = 0 yield surface
G = 0 potential surface
H hardening parameter
$\sigma_{ij}$ stress tensor.

The plastic compressive model uses the spherical cap yield surface proposed by Lade (7) with an associated flow rule. The governing parameters are best represented through isotropic loading and unloading tests with the elastic strain components eliminated to give:

$$v^c = B(\frac{s}{p_A})^{BP} \qquad (5)$$

The level of complexity intensifies in the plastic deviatoric model. In the triaxial plane, the failure surface passes through the origin and is curved, reflecting the reduction in friction angle with increased isotropic stress level. The equation of this surface is given by:

$$(\frac{t_f}{p_A}) = C(\frac{s_f}{p_A})^{CP} \qquad (6)$$

where if CP = 1, as for very loose materials, a straight failure surface is obtained analogous to Mohr-Coulomb.

In this case:

$$C = \frac{2\sqrt{2}\sin\phi}{3 - \sin\phi} \qquad (7)$$

or $$\phi = \arcsin(\frac{3C}{2\sqrt{2} + C}) \qquad (8)$$

The failure surface represents the outermost of a family of yield surfaces of similar shape.

The potential surfaces are non-associated and of the stress-dilatancy type, eg. Rowe (12), thus the deviatoric model is capable of giving compressive strains for shear stress levels below the threshold value at which dilation commences. The threshold shear stress level, equivalent to a mobilised friction angle $\phi_f$, varies with isotropic stress level, but always lies in the range:

$$\phi_\mu \leq \phi_f \leq \phi_{cv} . \qquad (9)$$

This implies that for quartz sand for example, $\phi_f \simeq 30^o$ but can vary by up to about $7^o$.

The yield and failure surfaces in the pi-plane are as those described by Lade and Duncan (17), whence

$$F = \frac{I_1^3}{I_3} - 27 - f_d = 0 \qquad (10)$$

where $I_1 = \sqrt{3}\, s$

$I_3 = \sigma_1\sigma_2\sigma_3$

and $f_d$ is a measure of the extent of the yield surface.

At failure, this surface agrees with Mohr-Coulomb in triaxial compression where

$$(\frac{I_1^3}{I_3})_f = (\frac{K_p + 2}{K_p})^3 \qquad (11)$$

and $K_p = \tan^2(45^o + \phi/2)$.

In triaxial extension, however, it predicts a higher stress ratio at failure than Mohr-Coulomb.

The potentials in the pi-plane are similar in form to those proposed by Lade and Duncan (17) but a parameter RT enables a modification to be made to their shape. When RT = 1, Lade and Duncan's original potentials are retrieved, whereas RT = $0^+$ gives a circular surface in the pi-plane. In the present work, RT = 0.3 has been used in line with experimental observations of Yamada and Ishihara (15).

## FINITE ELEMENT IMPLEMENTATION

With a view to the eventual solution of boundary value problems, the performance of the soil model was observed by incorporating it in a finite element analysis. In the present work, a single two-dimensional element was considered. As seen in Fig.1, the element was a four-noded quadrilateral taking account of the axial symmetry of a triaxial sample and its plane of symmetry about the mid-height. For simplicity, the dimensions of the element were taken to be unity in both the radial and depth directions.

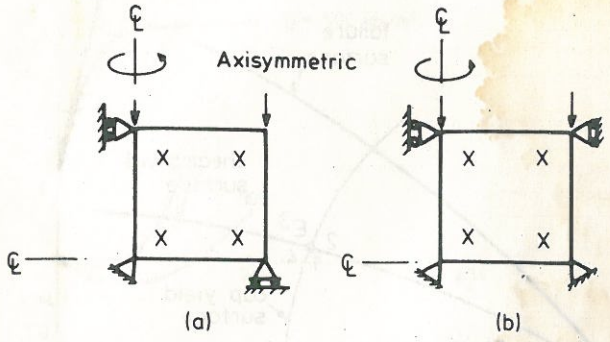


FINITE ELEMENT BOUNDARY CONDITIONS FOR
(a) TRIAXIAL LOADING (b) KO LOADING

Fig.1

For the modelling of $K_o$ stress paths, an additional lateral restraint was necessary as seen in Fig.1(b) to maintain the zero lateral strain requirement.

Integration over the element, such as that required in the stiffness formulation was performed using two-point Gaussian quadrature which amounts to four integrating points per element. Although this level of quadrature would be "exact" for the four-noded quadrilateral element in plane strain, this is not the case in axisymmetry due to the singularity that occurs in the strain/displacement relation as $r \to 0$. A three-point scheme, for example, will give a greater stiffness in axisymmetry than the two-point scheme, but this did not make a significant difference in the present work.

All the results presented in this paper were obtained using load (or stress) controlled tests. That is to say the stress path to be traversed was known in advance where the loads to be applied could be treated as input data. The results obtained were the displacements and strains generated by the loads. A typical run would therefore involve the selection of a stress path, the reading in of the initial stress state, and the calculation of the strain increments (used to update the total strain) generated by each load increment.

Typical stress paths that can be considered are as follows:

(PC) Passive Compression – Constant cell pressure
Increasing axial stress

(PE) Passive Extension – Constant axial stress
Increasing cell pressure

(AC) Active Compression – Constant axial stress
Falling cell pressure

(AE) Active Extension – Constant cell pressure
Falling axial stress

(CR) Constant Stress Ratio $-\sigma_1'/\sigma_3' = \text{constant}$

(CM) Constant Mean Stress $-\sigma_1' + 2\sigma_3' = \text{constant}.$

The nodal forces that must be applied to reproduce any of the above stress paths should be given some consideration. In Fig.2, an axisymmetric element which has finite internal and external radii, is subjected to increments of stress $\Delta\sigma_z$ and $\Delta\sigma_r$ in the vertical and radial directions. It can be shown that for this element, the consistent nodal forces equivalent to

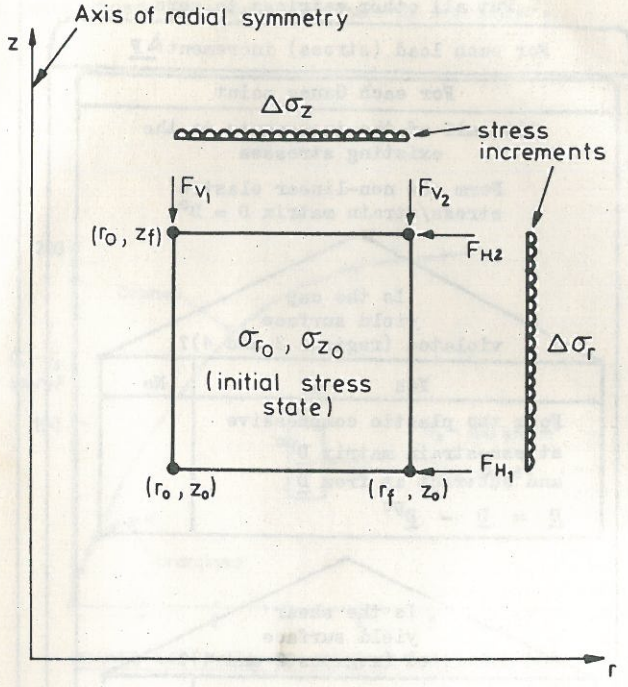


CONSISTENT NODAL FORCES IN AXISYMMETRY

Fig.2

these uniform stresses are given by:

$$F_{V_1} = \Delta\sigma_z \frac{(r_f - r_o)}{6}(2r_o + r_f) \tag{12}$$

$$F_{V_2} = \Delta\sigma_z \frac{(r_f - r_o)}{6}(r_o + 2r_f) \tag{13}$$

$$F_{H_1} = F_{H_2} = \Delta\sigma_r \frac{(z_f - z_o)}{2} \tag{14}$$

where these forces act over one radian.

In the present work where

$$r_o = z_o = 0, \qquad r_f = z_f = 1,$$

these expressions simplify to:

$$F_{V_1} = \Delta\sigma_z/6 \tag{15}$$

$$F_{V_2} = \Delta\sigma_z/3 \tag{16}$$

$$F_{H_1} = F_{H_2} = \Delta\sigma_r/2 \tag{17}$$

The solution algorithm involves re-calculating the structure stiffness matrix at each load step due to the stress-strain matrix $\underline{D}$ being itself a function of stress. Thus the method amounts to a tangent modulus approach with simple Euler extrapolation at each step. Errors due to this simple numerical technique were checked at all times by observing the influence of load step size on computed results.

The following structure chart shows the main logic flow of the solution method used here. As stated previously, in stress controlled tests the portion of stress space being traversed is known in advance. For example, in Fig.3 a "PC" test would require incorporation of both plastic matrices, whereas an "AC" test would only require the plastic deviatoric

read in model parameters,
initial stress state,
required stress path.
Put all other matrices to zero

For each load (stress) increment $\underline{\Delta F}$

For each Gauss point

Add half of the increments to the existing stresses

Form the non-linear elastic stress/strain matrix $D = D^e$

Is the cap yield surface violated (regions 3 and 4)?

| Yes | No |
|---|---|
| Form the plastic compressive stress-strain matrix $\underline{D}^{pc}$ and subtract it from $\underline{D}$ $\underline{D} = \underline{D} - \underline{D}^{pc}$ | |

Is the shear yield surface violated (regions 2 and 4)?

| Yes | No |
|---|---|
| Form the plastic deviatoric stress strain matrix $\underline{D}^{pd}$ and subtract it from $\underline{D}$ $\underline{D} = \underline{D} - \underline{D}^{pd}$ | |

Store the $\underline{D}$ matrix

Form the strain displacement relation $\underline{B}$ at that Gauss point

Form $\underline{B}^T \underline{D} \underline{B}.r$, multiply it by its quadrature weighting and add into the element stiffness matrix $\underline{K}$

Solve for nodal displacement increments $\underline{\delta}$ in

$$\underline{\Delta F} = \underline{K}\,\underline{\delta}$$

For each Gauss point

Form the strain displacement relation $\underline{B}$

Obtain strain increments

$$\underline{\Delta\varepsilon} = \underline{B}\,\underline{\delta}$$

Retrieve the $\underline{D}$ matrix

Obtain the stress increments

$$\underline{\Delta\sigma} = D\,\underline{\Delta\varepsilon}$$

Update strains and stresses

$$\underline{\varepsilon} = \underline{\varepsilon} + \underline{\Delta\varepsilon}$$

$$\underline{\sigma} = \underline{\sigma} + \underline{\Delta\sigma}$$

Update displacements

$$\underline{d} = \underline{d} + \underline{\delta}$$

Print results

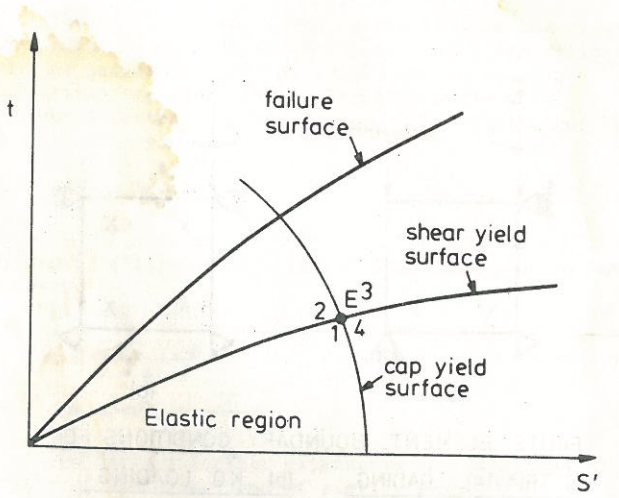


YIELD AND FAILURE SURFACES IN STRESS SPACE

Fig.3

matrix, the cap not coming into play. Triaxial unloading on the other hand would use the non-linear elastic matrix only.

In more complicated boundary value problems, the direction and the extent to which a particular stress increment at a given Gauss point has violated a yield surface will not be immediately apparent. Extra calculation is then necessary to establish the region of stress space that is being traversed. If it is found that a particular stress probe has only partially violated a yield surface, the magnitude of the plastic stress-strain matrix concerned should be reduced proportionately.

## DRAINED STRESS PATHS

This aspect of the model behaviour has been considered previously (5) in some detail and so is only mentioned briefly here ($K_o$ conditions are dealt with separately below). Typical results are shown in Fig.4 for medium dense sand in triaxial tests at varying cell pressure. In terms of stress ratio, the higher cell pressures 'weaken' the soil causing suppression of dilatancy and the tendency for dense material to behave more like loose. An aspect of the behaviour of sand which is extremely important is illustrated in Fig.5. When compressed at constant stress ratio, dense sands decrease in volume for low stress ratios but increase in volume for higher stress ratios. This has vital implications for "density hardening" models such as "Cam clay" because clearly dense sand can "density soften" although in any other measure of work it is hardening. For this reason the authors reject "Cam clay" as a useful basis for a general description of soil (16).

## UNDRAINED STRESS PATHS

This is a greater potential area for the use of the more complicated soil models. Small perturbations in the porewater pressures in loose undrained sands (due to upward percolation of water, small impacts etc) can cause the soil strength to decrease essentially to zero ("liquefaction"). Some undrained stress paths for very loose sand are shown in Fig.6.

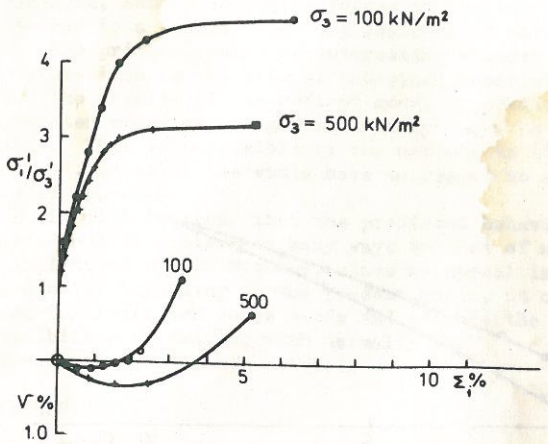


DRAINED STRESS/STRAIN BEHAVIOUR OF MEDIUM DENSE SAND

Fig.4

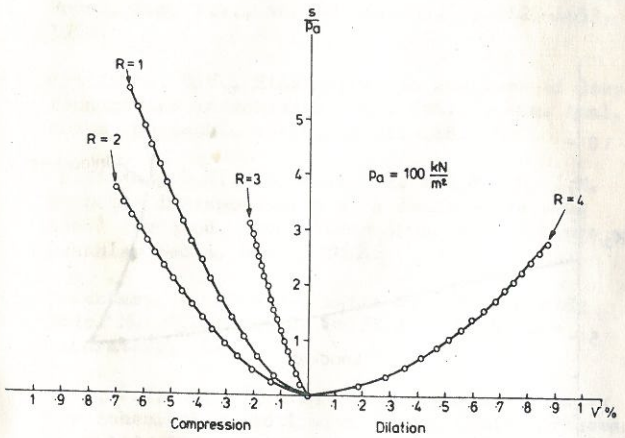


VOLUMETRIC STRAINS DUE TO CONSTANT R PATHS

Fig.5

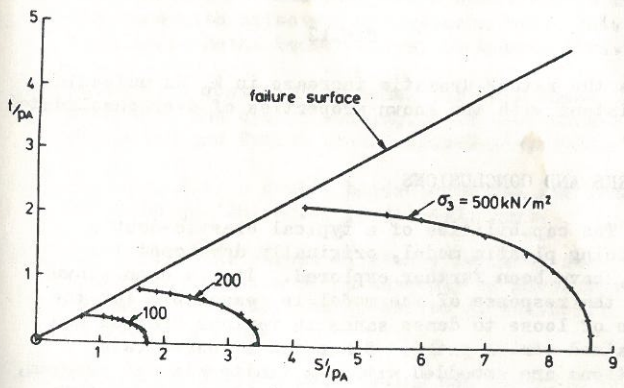


UNDRAINED STRESS PATHS FOR VERY LOOSE SAND

Fig.6

Here the failure surface coincides with the $\phi_{cv}$ line and no dilation occurs. Thus the soil has no reserve of strength to withstand the greater strains caused by any increase in porewater pressure. Fig.7 shows the drained and undrained responses of the same soil in triaxial tests at a cell pressure of 100 kN/m$^2$.

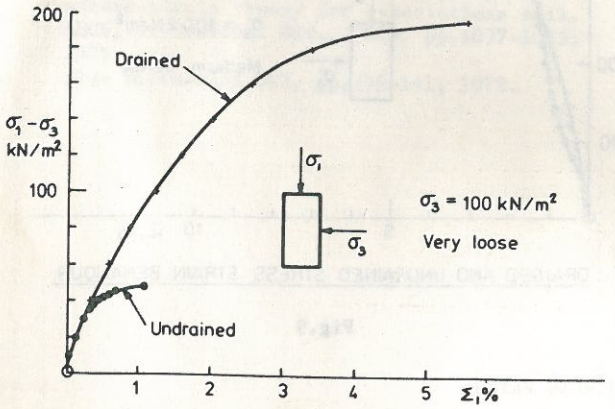


DRAINED AND UNDRAINED STRESS/STRAIN BEHAVIOUR

Fig.7

Contrasting behaviour for medium dense sand is shown in Figs.8 and 9. Fig.8 shows the strengthening stress paths followed by undrained specimens and Fig.9 shows that in the absence of cavitation or attainment of critical confining pressure, the undrained specimen of medium dense sand would have a higher strength than its drained counterpart.

These computations for undrained soil were conducted by adding a "large" bulk stiffness to the effective soil stiffness matrix in the usual manner. The response is insensitive to precisely how large the added bulk stiffness is.

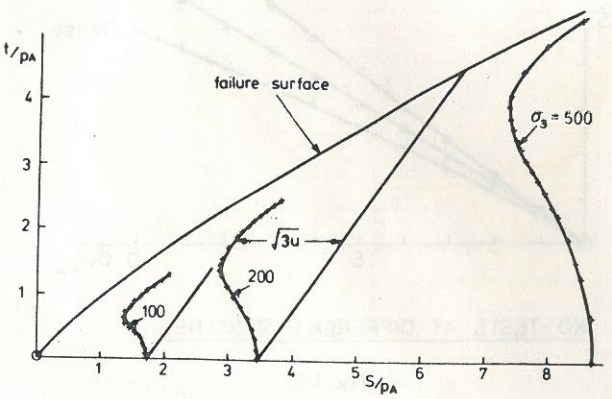


UNDRAINED STRESS PATHS FOR MEDIUM DENSE SAND

Fig.8

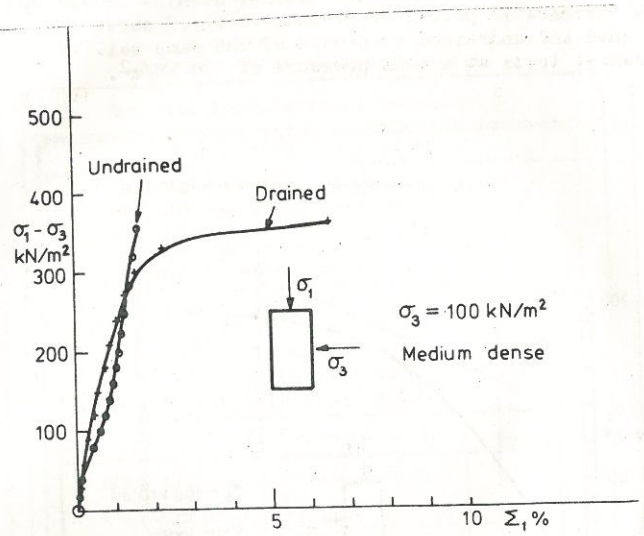


DRAINED AND UNDRAINED STRESS STRAIN BEHAVIOUR

Fig.9

## $K_o$ STRESS PATHS

An important feature of soil is its behaviour in conditions of consolidation or swelling under zero total lateral strain. In early treatments such as "modified Cam clay" attempts were made to deal with the $K_o$ condition by plasticity formulations alone whereas the reality involves a complex interaction of elastic and plastic strains. The double hardening elastic-plastic model should therefore be capable of describing $K_o$ behaviour.

Results of calculations for three soil densities are shown in Fig.10. It can be seen that the predicted responses are reasonable, with $K_o$ increasing as the soil gets looser.

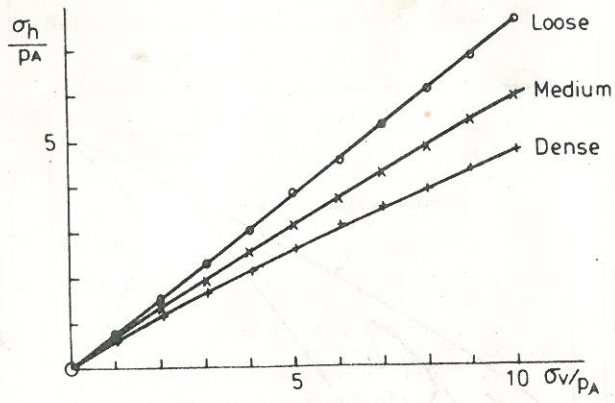


KO-TESTS AT DIFFERENT DENSITIES

Fig.10

Results for dense sand are replotted in different ways in Figs.11 and 12. Fig.11 agrees well with the shape of published curves from laboratory tests while Fig.12

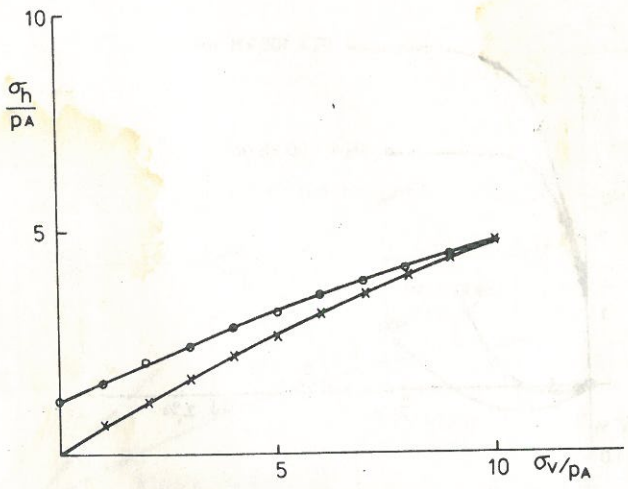


KO LOADING / UNLOADING ON DENSE SAND

Fig.11

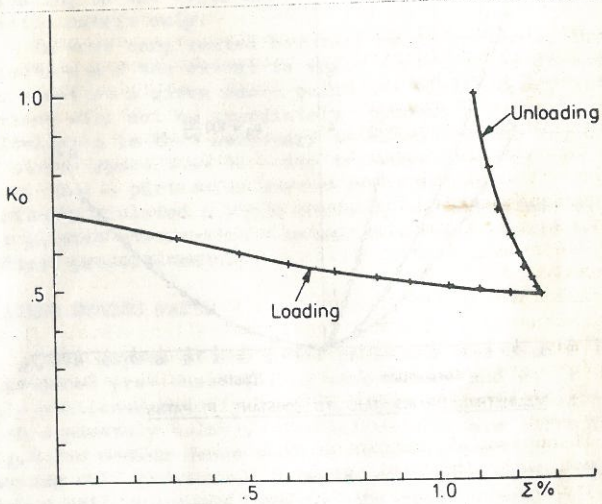


VARIATION IN KO FOR DENSE SAND

Fig.12

shows the rather dramatic increase in $K_o$ on unloading, consistent with the known properties of overconsolidated soil.

## REMARKS AND CONCLUSIONS

The capabilities of a typical elastic-double hardening plastic model, originally developed for sand, have been further explored. It has been shown that the response of the model is reasonable for the range of loose to dense sands in various drained and undrained stress paths. Since the stress-strain equations are embedded within a finite element program, extrapolation to boundary value problems is feasible. However a priority is to establish which boundary value problems would benefit from such a detailed treatment. The writers believe that most problems involving drained soils can be satisfactorily

analysed using simpler models, eg. (3) or (4). However, the $K_o$ results presented in this paper could not be reproduced using the simpler constitutive laws. Therefore, some problems of forces on buried structures adjacent to a loaded structure could be of interest.

The primary source of interesting boundary value problems lies in the area of undrained behaviour. Here the ability of the refined model to predict porewater pressure changes accurately could be of great value. This is impossible by the methods in (3) for example, in which one would have to resort to a total stress approach.

It will be clear that the predicted behaviour of loose sand is similar in many ways to that of normally consolidated clay. However, since no appeal is made to density hardening in the present model, it can be used for loose and dense sands and affords the possibility of dealing with normally and overconsolidated clays as well.

REFERENCES


(1) Pande, G.N. and Zienkiewicz, O.C. (eds). Soil Mechanics-Transient and Cyclic Loads, Wiley, 1982.

(2) Yong, R.K. and Ko, H.K. (eds). Limit equilibrium, plasticity and stress-strain in geotechnical engineering, ASCE, 1981.

(3) Duncan, J.M. and Chang, C.Y. Non-linear analysis of stress and strain in soils. ASCE, J. Soil Mech. Found. Eng. Div., vol.96, No.SM5, pp.1629-1653, 1970.

(4) Griffiths, D.V., Elasto-plastic analyses of deep foundations in cohesive soil. Int. J. Num. Anal. Meths. Geomech., vol.6, pp.211-218, 1982.

(5) Griffiths, D.V., Molenkamp, F. and Smith, I.M. Computer implementation of a double-hardening model for sand. Proc. IUTAM Symp. Def. Failure of Granular Media, Delft, 1982.

(6) Molenkamp, F. Elasto-plastic double hardening model MONOT, Report of Delft Soil Mechanics Laboratory, 1981.

(7) Lade, P.V., Elasto-plastic stress-strain theory for cohesionless soil with curved yield surfaces. J. Solids Structures, vol.13, pp.1019-1035, 1977.

(8) Ghaboussi, J. and Momen, H. Modelling analysis of cyclic behaviour of sands, Soil Mechanics-Transient and Cyclic Loads, pp.313-342, 1982.

(9) Mroz, Z. and Pietruszczak, S. A constitutive model for sand with anisotropic hardening rule. Int. J. Num. Anal. Meth. Geomechanics, to appear 1983.

(10) Nova, R. A constitutive model for soil under monotonic and cyclic loading. Soil Mechanics-Transient and Cyclic Loads, pp.343-374, 1982.

(11) Vermeer, P.A. A double hardening model for sand, Geotechnique 28, No.4, pp.413-433, 1978.

(12) Rowe, P.W. The stress dilatancy relation for static equilibrium of an assembly of particles in contact. Proc. Roy. Soc., Series A, Vol.269, pp.500-527, 1962.

(13) Rowe, P.W. Theoretical meaning and observed values of deformation parameters for soil, Proc. Roscoe Mem. Symp. Cambridge, pp.143-194, 1971.

(14) Tatsuoka, F. and Ishihara, K. Yielding of sand in triaxial compression. Soils and Fnds., vol.14, No.2, pp.63-76, 1974.

(15) Yamada, Y. and Ishihara, K. Anisotropic deformation characteristics of sand under three-dimensional stress conditions. Soils and Fnds., vol.19, No.2, pp.79-94, 1979.

(16) Smith, I.M. Plane plastic deformation of soil. Stress-strain Behaviour of Soils (ed Parry), pp.548-563, Foulis, 1971.

(17) Lade, P.V. and Duncan, J.M. Elasto-plastic stress-strain theory for cohesionless soil. ASCE, J. Geotech. Div., GT10, pp.1037-1053, 1975.
Also Discussion GT3, pp.139-141, 1978.